Processing and Application of Ceramics 13 [1] (2019) 1–11
https://doi.org/10.2298/PAC1901001D

Structure, dielectric and electrical properties of relaxor lead-free double perovskite: Nd_2NiMnO_6

Rutuparna Das*, Ram Naresh Prasad Choudhary

Department of Physics, Siksha O Anusandhan (Deemed to be University), Bhubaneswar-751030, India

Received 8 June 2018; Received in revised form 14 September 2018; Accepted 19 November 2018

Abstract

In this paper, dielectric relaxor, impedance, AC conductivity and electrical modulus of double perovskite Nd_2NiMnO_6, prepared by a solid state reaction method and sintered at 1250 °C, have been reported in the wide temperature (25–150 °C) and frequency (1 kHz–1 MHz) ranges. From the preliminary X-ray structural analysis, it is found that the structure of the material is monoclinic. In the study of the temperature dependence of the dielectric constant, the relaxor behaviour of the material is observed. Such type of behaviour is explained by a modified Curie-Weiss and a Vogel-Fulcher law. By analysing Nyquist plots, the existence of grain and grain boundary effects is established. The non-Debye type of relaxation is investigated by the analysis of complex impedance and the modulus data. From the study of impedance data, it is found that the grain resistance is reduced with the increase in temperature indicating the existence of negative temperature coefficient of resistance (NTCR) behaviour in the material which also matches with temperature versus AC conductivity plots. From these results, it may be concluded that this compound may have extreme potential for different high temperature applications.

Keywords: *Nd_2NiMnO_6, solid state reaction, XRD, dielectric, relaxor behaviour*

I. Introduction

In the last decade, there is an enormous importance in producing novel magneto-electric multiferroics, which are the most significant for their practical application in spintronics and magneto-electric devices [1]. Such type of materials has been found in different structural families, including perovskite. Multiferroic oxides can also be found in the class of double perovskite materials. The perovskite structure compounds are significant in materials science, and have been broadly studied in recent years. Their structural characteristics are very important for application in telecommunication and microelectronics. Thus, it is well identified that distortion in the structure, vacancies and modifications in composition can lead to different chemical and physical properties [2]. When two dissimilar kinds of cations are added at the octahedral position of an ideal perovskite structure (XYO_3) then the ordering of cations results in the cubic complex perovskite known as double perovskite with a common formula $X_2YY'O_6$, where X is an alkaline earth or rare earth ion and Y and Y′ are transition metals. They display different features like insulating, metallic, ferromagnetic, magneto-dielectric, multiferroic etc. [3]. The ideal perovskite systems are highly symmetric, and the oxygen atoms are located between Y and Y′ ions on a straight line. Structural deformation results in the tilting of the $YO_6/Y'O_6$ octahedra that affects the interactions along the Y−O−Y′−O−Y paths, providing different functional properties.

Multiferroic double perovskite materials exhibit different ferroic ordering in a single phase [4]. The charge ordering, distortion in the octahedra, strain mediation, lone-pair of electrons and geometrical frustration are mainly origins of ferroelectricity in a material and vacant *d*-orbital is required. However, the origin of magnetism in a ferromagnetic material is linked with the ordering of spins of electrons and it requires partially filled *d*-orbital. The structure of double perovskite material can be predicted from the tolerance factor. The acceptable level of tolerance of double perovskite, usually referred to as the tolerance factor (t'), can be estimated by using a simple equation:

*Corresponding authors: tel: +91 77 5087 9683,
e-mail: *rutulucy2013@gmail.com*

$$t' = \frac{r_x + r_O}{\sqrt{2}\left(\frac{r_y + r_{y'}}{2} + r_O\right)} \quad (1)$$

where r_x, r_y, $r_{y'}$, r_O are the ionic radii of X, Y, Y′, cations and oxygen anion, respectively. For $t' < 1$, there is distortion in symmetry, i.e. structure will be tetragonal or monoclinic [5].

R_2NiMnO_6 (R is a rare earth cation) belongs to a specific class of double perovskite oxides. Ni–O–Mn adjustment may arise in inherent strong ferromagnetic interaction, thus it could be considered as an excellent candidate for multiferroic materials. For instance, in recent times it has been revealed that the occurrence of magneto-resistance and giant dielectric properties, excluding the ferromagnetism, are owing to the Ni^{3+}–O–Mn^{3+} super exchange interactions, while Blasse *et al.* [6] aspect the ferromagnetism totally due to the Ni^{2+}–O–Mn^{4+} super exchange interactions. It is also revealed that the giant dielectric properties arise from the ordering of charge between Ni^{2+} and Mn^{4+}. Therefore, the discussion related to the Ni–O–Mn electronic interactions suggests that the presence of R_2NiMnO_6 group is an increasing issue in the last years. Also, for industrial applications, the excellent characteristic of this compound is its performance in a low magnetic field at room temperature [6,7]. Since Mn ions exist in multi-valence states (Mn^{2+}, Mn^{3+} and Mn^{4+}) MnO_2 is generally used as the most convenient additive. Manganese containing rare earth based double perovskite (with multiple functions) can be used for different devices [8]. A significant magneto-dielectric effect can be observed in the double perovskite ferromagnet La_2NiMnO_6. In such type of material, the super-exchange interaction between Ni^{2+} and Mn^{4+} ions by means of an oxygen gives the ferromagnetic transition at $T = 270$ K [9]. Specially, a material showing a huge energy loss (tangent loss) may lead to an extraordinary magneto-dielectric effect, widely established as the Maxwell-Wagner effect, occurring due to the existence of material-electrode interface and/or grain boundaries [10–12]. Therefore, it is required to find the way to reduce the energy loss in such type of magnetic materials for practical applications, which can be achieved by modification of the materials.

The dielectric relaxation phenomena and its origin have been studied in different double perovskite systems [13]. The complexity in the structure of perovskite compound is created by more than one ion which are totally or fractionally disarranged in the X and Y sublattices of the XYO_3 structure [14]. Based on the relaxation process, disorderness and/or fluctuation of charge of elements at different atomic sites, particularly at Y sites, create a few types of ferroelectrics, referred to as relaxor ferroelectrics. The high dielectric constant is one of the main features of ferroelectrics. Generally, in 'normal' ferroelectrics, maximum temperature dielectric constant (T_m) signifies the ferroelectric-paraelectric (FE-PE) phase transition temperature (T_C) [15]. In the vision of the significance of the materials, we have carried out preparation and characterization of a double perovskite (Nd_2NiMnO_6) using various experimental techniques as a function of frequencies and temperature. Studies of the diffused phase transition (DPT) as well as relaxor properties in the materials are carried out for both fundamental understanding and technological applications. Therefore, relaxor ferroelectrics (RFEs) have been extensively studied for their exceptionally higher dielectric constant and attractive piezoelectric properties, which are essential for high-energy density capacitors and actuators. Such types of materials may be used for non-volatile memories, sensors, actuators, resonant wave devices such as radio-frequency filters, infra-red detectors, optical switches and electric-motor overload protection circuits [16].

II. Experimental procedure

The polycrystalline Nd_2NiMnO_6 (NNMO) compound has been fabricated at high temperature by mixed oxide method using pure oxide ingredients: Nd_2O_3, MnO_2 (99.9% pure, supplied by Loba Chemie Co. Ltd) and NiO (99.5% pure supplied by Himedia) in the stoichiometry ratio. To obtain homogeneous mixture, the fine precursor powders were mixed properly by dry grinding as well as wet grinding in methanol by a mortar and pestle. To confirm the completion of the chemical reaction and formation of required compound, calcinations (750–1200 °C with the interval 50 °C) and grinding processes were repeated ten times. Accordingly, calcination temperature of 1200 °C and dwell time of 4 h were selected. Then, the cylindrical pellets of diameter 10.70 mm and thickness 1.65 mm were fabricated using polyvinyl alcohol (PVA) as a binder under the pressure of about 4×10^6 N/m^2 using a hydraulic press. The sintering of the pellet was carried out at 1250 °C for 4 h.

The room temperature X-ray diffraction (XRD) data of the calcined powder were recorded with CuKα radiation ($\lambda = 1.5406$ Å) in a scattering angle range $20° \leq 2\theta \leq 80°$ for preliminary structural analyses (crystal system, lattice constant of unit cell, diffraction planes, etc.). The structural analysis was carried out using software "POWDMULT" (version 2.2). The microstructure of the sintered pellet was analysed by a field emission scanning electron microscope (FE-SEM, M/s ZEISS, model SUPRA 40). Elemental composition was determined from EDAX (energy dispersive X-ray analysis) spectra. Both sides of the sintered pellet were polished and coated with the high-purity silver paste. The pellet was heated at 120 °C for 4 h to make moisture free material for electrical measurements. The dielectric properties, impedance, electrical conductivity, etc. of the silver electrode-pellet sample were measured by using an LCR meter (N4L PSM, 1735) in a wide range of temperature (25–150 °C) and frequency (1 kHz–1 MHz).

III. Results and discussion

3.1. Structure

After calcination and grinding processes, XRD pattern (Fig. 1) was obtained. According to the tolerance factor, members of the double perovskite family have different structure, such as: i) cubic for $1.05 > t' > 1.00$, ii) tetragonal for $1.00 > t' > 0.97$, and iii) monoclinic/orthorhombic for $t' < 0.9$. As the determined tolerance factor (using the above equation) of Nd_2NiMnO_6 is less than 0.97, it might have orthorhombic or monoclinic symmetry. The reported crystal symmetry of other rare-earth compounds of this family with equal tolerance factor is monoclinic. The peaks of the XRD pattern of Nd_2NiMnO_6 were indexed as monoclinic as well as orthorhombic crystal system using software "POWDMULT". The determined lattice constants of the monoclinic (distorted double-perovskite) structure are: a = 7.0820(55) Å, b = 5.1626(55) Å and c = 5.5876(55) Å, β = 103.59° and V = 198.56 Å^3 (number in the parenthesis of the cell parameter is estimated standard deviation). The observed XRD pattern and obtained lattice parameters are very much similar and consistent with the reported ones [17]. The crystallite size (D) of the sample can broadly be determined by using peak broadening, scattering angle, wavelength, and optimized constant of diffraction peaks in Scherrer's equation [18,19]. The determined D value is 41 nm and density of the sample is 4.78 g/cm^3. As the XRD pattern is recorded on the powder sample, a mechanical strain component of the equation was not estimated.

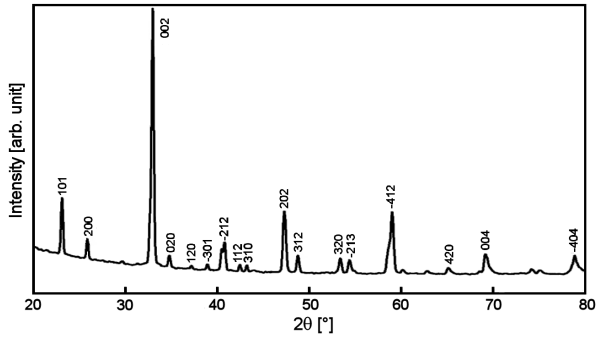

Figure 1. XRD pattern of calcined Nd_2NiMnO_6 powder

Figure 2 represents FE-SEM microstructure of the sintered NNMO pellet. The image shows the different size of grains which are scattered homogeneously suggesting the polycrystalline nature of the compound. The nature of grain shape and distribution clearly suggests that material is highly dense, free from pores and with the average grain size of ~0.3 μm. Elemental composition determined by EDX spectrum analysis was given in Table 1. The EDAX spectra verified the existence of necessary elements (i.e. Nd, Ni, Mn and O elements) without any foreign elements in the sample.

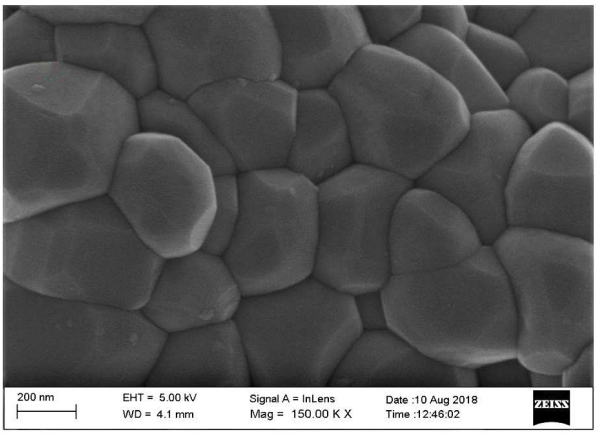

Figure 2. FE-SEM micrograph of the sintered Nd_2NiMnO_6 ceramics

Table 1. Elemental composition of sintered Nd_2NiMnO_6 ceramics

Element	Composition	
	[wt.%]	[at.%]
O K	20.52	62.83
Mn K	10.54	9.40
Ni K	8.79	7.34
Nd L	60.15	20.43

3.2. Dielectric studies

Effect of frequency

Variations of relative dielectric constant, ε_r, and tangent loss, tan δ (two fundamental parameters of a dielectric material) [15], with the frequency at selected temperature for Nd_2NiMnO_6 are displayed in Fig. 3. Both ε_r and tan δ are continuously reduced and attain a consistent value in the high-frequency region with the increment of frequency describing the main features of the polar dielectrics [20,21]. It is seen that the material has very large dielectric constant (8×10^3) at 1 kHz because of the existence of different types of polarizations (i.e. ionic, dipolar or orientation, electronic and space charge) in the low-frequency region. The dielectric constant after 1 kHz exhibits a plateau [22] having a large temperature dependence above 75 °C. Depending on the two-layer model of Koop's phenomenological hypothesis, Maxwell-Wagner proposed a mechanism which explains decreasing trend of both ε_r and tan δ with the increment of frequency. At low frequencies, the dielectric loss rises naturally with an increment of temperature, referred to the increase of DC conductivity in Nd_2NiMnO_6 apparently due to the hopping of electrons between Mn^{3+} and Mn^{4+}. The grains are extremely conducting as compared to the grain boundaries. Only at low-frequency, the passage of charge carriers to the grain boundary produces a huge amount of energy loss. As it is well known, dielectric loss means the extent of energy used by the applied field for the alignment of dipoles. Dielectric loss in perovskite ox-

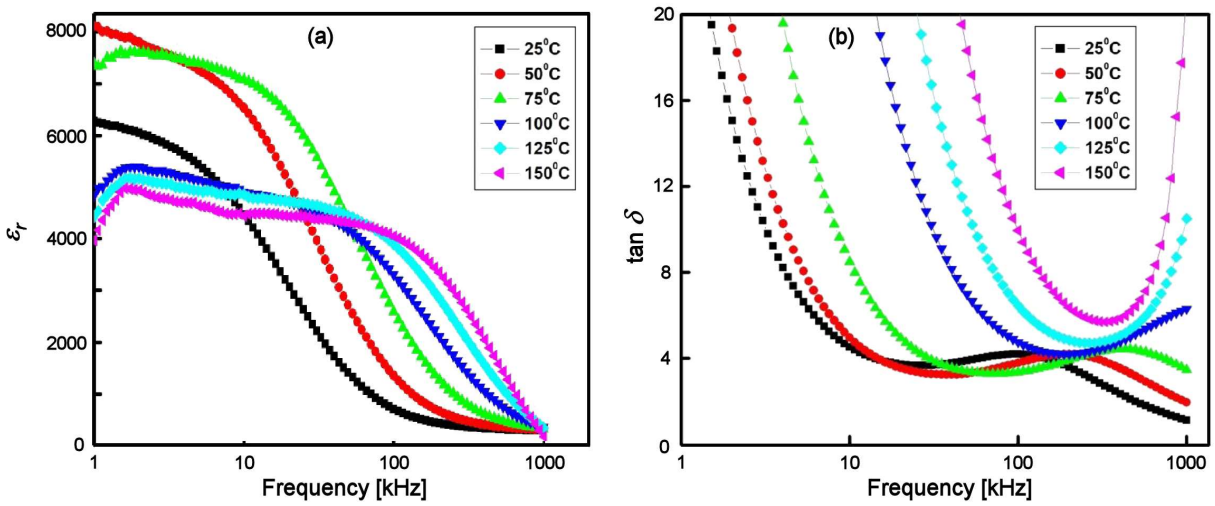

Figure 3. Change of dielectric constant (a) and dielectric loss (b) with frequency for Nd_2NiMnO_6 ceramics

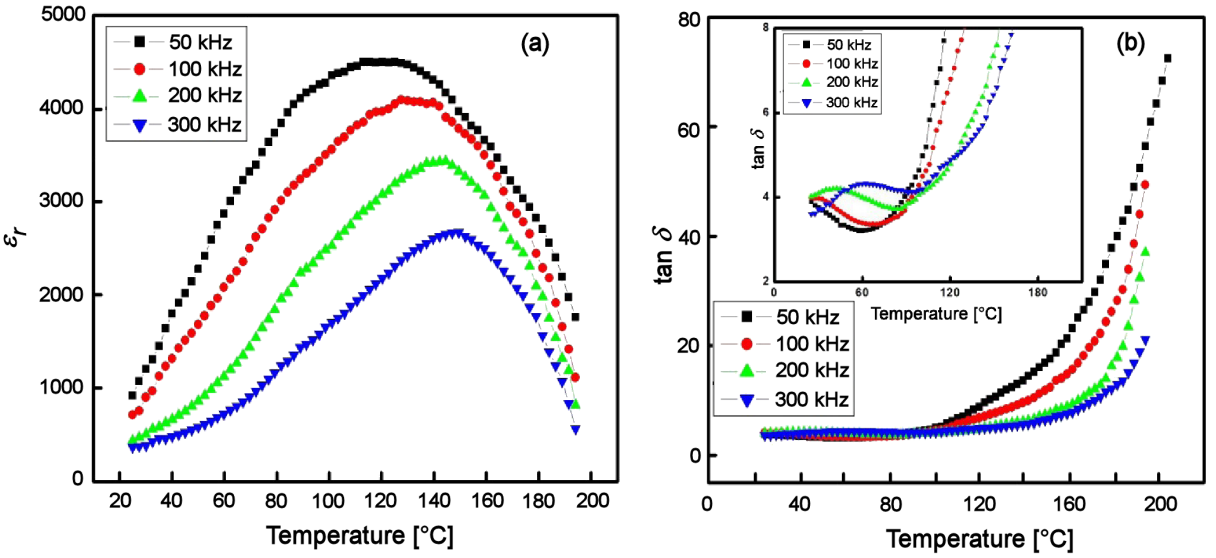

Figure 4. Change of dielectric constant (a) and dielectric loss (b) with temperature for Nd_2NiMnO_6 ceramics

ides is caused by DC conductivity and oxygen vacancies. At high temperatures, the value of high-frequency $\tan\delta$ is large which is due to the scattering of thermally induced charge carriers and the existence of several unknown defects (counting oxygen vacancies) in the material. At high temperatures, the domination of conductivity is responsible for the rise in $\tan\delta$. Therefore, in this region, $\tan\delta$ is high in comparison to that of the low-frequency region.

Effect of temperature

Variations of relative dielectric constant (ε_r) and tangent loss ($\tan\delta$) with temperature at certain frequencies of the sintered Nd_2NiMnO_6 sample are depicted in Fig. 4. It can be noticed that ε_r rises up to the maximum and then decreases. Dielectric anomaly or peak is observed at different temperature on changing frequency. The shifting of dielectric peak towards higher temperatures with an increment of frequency is referred to as the dielectric relaxation. Such type of peak shifting and coinciding the value of relative dielectric constant provides an interesting class of ferroelectric family, referred to as relaxor ferroelectrics. The larger value of ε_r is viewed in the low-frequency (50 kHz) region because of the gathering of charge near the grain boundaries. At low-temperatures, the value of $\tan\delta$ is low, but when temperature increases, the value of $\tan\delta$ increases to very high values. The scattering of charge carriers and defect/vacancies created during the high temperature process may be responsible for the sharp increment in $\tan\delta$ at high temperatures. Not only this, but electrical conductivity is also responsible for such type of variation.

Inset in Fig. 4b shows precisely the broad peak in dielectric loss curves. The peak in $\tan\delta$ is shifted to high temperatures with the increment of frequency. Because of an increase of electrical conductivity, $\tan\delta$ rises more rapidly at high temperatures [18].

Dielectric relaxor behaviour

The origin of the observed relaxor behaviour has been accompanied with disorder of cations at the X or Y sites of the perovskite structure that prevents the development of the long-range polar ordering. Thus, some notable character of the dielectric relaxor materials can be described in such a way that: i) they are identified by large peaks in the temperature dependent dielectric permittivity curve, ii) the corresponding temperature of the maximum value of real and imaginary part of the dielectric constant having different values, presenting a frequency dependent behaviour, and iii) the Curie-Weiss law is not satisfied by temperatures about T_m [23]. It is known that "normal" ferroelectrics should obey the Curie-Weiss law expressed by:

$$\varepsilon = \frac{T_C}{T - T_C} \quad (T > T_C) \tag{2}$$

All the symbols have their usual meaning. The deviation from Curie-Weiss law is found (Fig. 5a) and it is measured by the parameter ΔT_m ($\Delta T_m = T_C - T_m$). The determined T_C values from the Curie-Weiss fit are 139.6, 160.3 and 175.6 °C at 50, 100 and 200 kHz respectively. The calculated values of ΔT_m are 43.5, 42.4 and 38.4 °C at 50, 100 and 200 kHz, respectively. This value of ΔT_m represents the extent of departure from the Curie-Weiss law. In Fig. 4a, there are broad peaks (with diffused phase transition) that are the important features of ferroelectric relaxor. Relaxor ferroelectric is characterized by a broad maximum along with relaxation dispersion in the curve of temperature versus dielectric permittivity. The ferroelectric diffused phase transition is explained by a frequency-independent temperature of maximum permittivity (T_m), while a relaxor ferroelectric is found to have a frequency-dependent T_m satisfying Vogel-Fulcher relation [22,24]. In this case, at low-temperatures, the strong frequency dispersion in permittivity is found, whereas the high temperature permittivity is almost frequency independent. This kind of relaxor nature can be described by the modified Curie-Weiss law for better understanding of the diffused phase transition. Still the true origin of diffused phase transition (DFPT) is unclear. However, it is thought to be mainly related to defects in the materials, due to the compositional fluctuation, grain configuration, cation disorder, point defects and microscopic heterogeneities. The relaxor ferroelectrics should obey the modified Curie-Weiss law represented by:

$$\frac{1}{\varepsilon} - \frac{1}{\varepsilon_m} = \frac{(T - T_m)^\gamma}{C} \tag{3}$$

or

$$\ln\left(\frac{1}{\varepsilon} - \frac{1}{\varepsilon_m}\right) = \gamma \cdot \ln(T - T_m) - \ln C \tag{4}$$

where all the symbols have their usual meaning, γ is known as the diffusion coefficient and it lies between 1 (a normal ferroelectric) and 2 (an ideal relaxor ferroelectric) [25,26]. To observe the effect of the diffuse phase transition nature, the graph of $\ln(1/\varepsilon - 1/\varepsilon_m)$ *vs.* $\ln(T - T_m)$ for 50 kHz and 300 kHz are shown in Fig. 5b. The γ value can be calculated from the slope of the fitting curves which is obtained from linear relation. The rate of the diffuseness of the phase transformation can be determined by exponent γ. We obtained the value of γ to be 2.03 and 2.04 at 50 kHz and 100 kHz, respectively, which is very close to 2 (as per reference [26]). This result suggests that Nd_2NiMnO_6 is a relaxor ferroelectric and its diffuseness increases with increment of frequency. In relaxor materials, relaxation behaviour can also be studied by the experimental Vogel-Fulcher (VF) model [27]. Such type of behaviour occurs due to the thermally activated polarization between two identical variants. The Vogel-Fulcher law is expressed by:

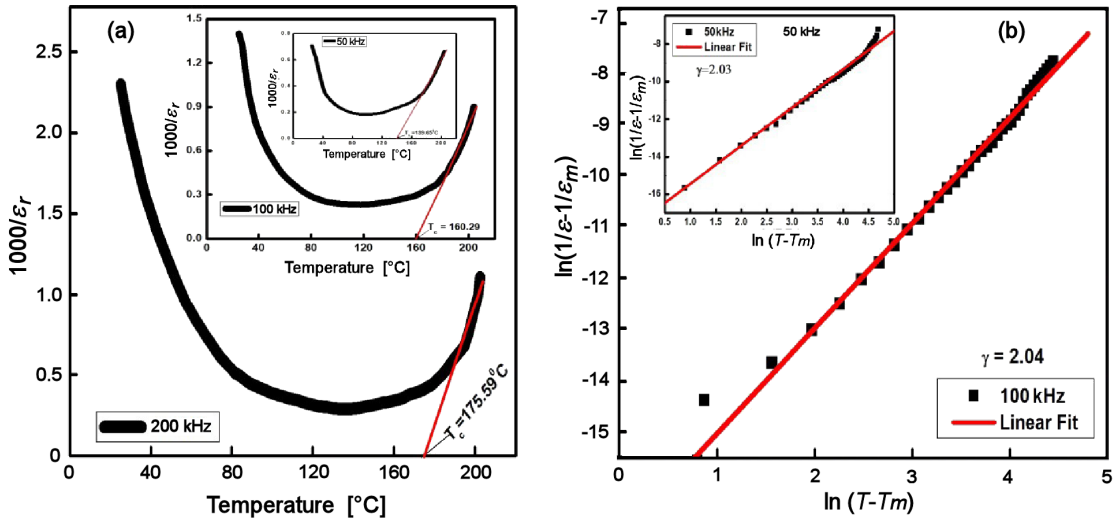

Figure 5. Inverse dielectric permittivity at 50 kHz, 100 kHz and 200 kHz as a function of temperature fitted according to the Curie-Weiss law (a) and plot of $\ln(1/\varepsilon - 1/\varepsilon_m)$ *vs.* $\ln(T - T_m)$ at 50 kHz and 100 kHz

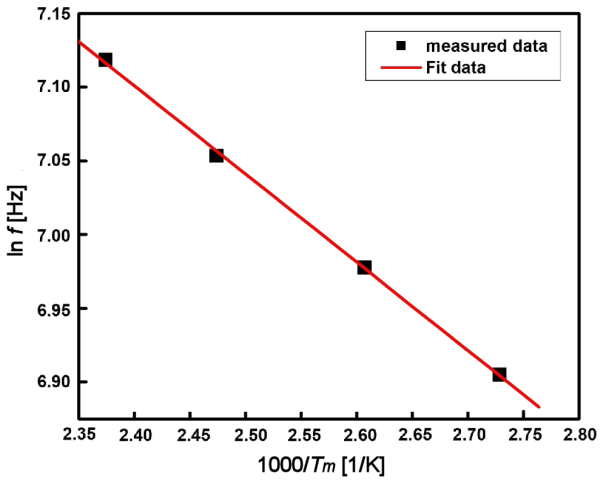

Figure 6. Graph of ln(f) with inverse of temperature (T_m)

$$f = f_0 \cdot \exp\left(\frac{-E_a}{k_B(T_m - T_f)}\right) \tag{5}$$

where all the symbols have their usual meaning. The freezing temperature (T_f) is a temperature at which the dynamic nature (generally produced by heat energy) is absent. Figure 6 is depicted as the graph of ln(f) with inverse of temperature (T_m). From the analysis of Vogel-Fulcher fitting, we found that activation energy and other parameters (E_a = 0.05 eV, f_0 = 5×10^3 Hz and T_f = 105 K with R^2 = 0.999) indicating that Nd_2NiMnO_6 exhibits relaxor behaviour. The energy needed for the displacement of an electron from Ni^{2+} to Mn^{4+} is the nearest to this estimated activation energy [28]. This activation energy is sufficient for switching over the orientation of polar regions. The arbitrarily dispersed electrical field of strain field in a mixed oxide system is the major logic for the appearance of relaxor behaviour [29]. Dielectric relaxation in the material may be caused by the hopping of polarons between Y and Y′ site cations, grain and grain boundary. This outcome is also related to the influence of conductivity due to the oxygen vacancies.

3.3. Impedance analysis

Complex impedance spectroscopy (CIS) method is associated with four elementary formalisms: impedance, admittance, permittivity and modulus formalism providing more data concerning the electrical behaviour of materials. To differentiate grain, grain boundary and electrode response of the material, the impedance measurement has been done. The passage of charges can appear in different form, especially displacement of charge (long-range or short-range), production of space charge and re-orientation of dipole etc. The measured complex impedance (Z^*) has both real (Z') and imaginary (Z'') components described by Eq. (6) and (7) [30–32]:

$$Z^* = Z' + j \cdot Z \tag{6}$$

$$Z' = \frac{R}{1 + (\omega \cdot \tau)^2} \quad \text{and} \quad Z'' = -\frac{\omega \cdot R \cdot \tau}{1 + (\omega \cdot \tau)^2} \tag{7}$$

where R is resistance of the sample, ω is angular frequency and $\tau = R \cdot C$ (C is the capacitance) is the relaxation time. The relaxation time is calculated by using an expression $\tau = R_g \cdot C_g$ (R_g is the effective resistance and C_g is the effective capacitance in parallel). The values of these parameters are given in Table 2. The Z' versus frequency graph is depicted in Fig. 7a. It is realized that Z' is almost stable up to 2 kHz and its value smoothly reduces when both frequency and temperature increase. The reduction of Z' is strongly dependent on frequency and temperature [33]. At lower frequencies, the reducing tendency of Z' value with temperature represents the negative temperature coefficient of resistance (NTCR) or semiconductor type behaviour representing semiconductor nature of the material. From the graph, it may be expected that the values of Z' will be merged for all temperatures above 1 MHz characterized by the liberation of space charge.

Figure 7b is depicted as the graph of Z'' versus frequency. From the plots it is realized that Z'' values reduce with increment of temperature. With increment of frequency the Z'' rises and at a particular frequency occurrence of a peak can be observed, known as relaxation frequency [34]. When temperature increases, there is a shift of the relaxation frequency in the high-frequency region with decrease in the peak height. It describes the existence of relaxation in the studied sample. The peak position yields the relaxation time from the relation $\omega_{max} \cdot \tau = 1$, where ω_{max} is the angular frequency of the Z''_{max}. The appearance of the temperature dependence of the relaxation phenomena is confirmed from the reduction of relaxation time with the rise in temper-

Table 2. Comparison of calculated values of grain resistance (R_g), grain boundary resistance (R_{gb}), grain capacitance (C_g), grain boundary capacitance (C_{gb}) and constant phase factor (Q_g, Q_{gb}) at some selected temperature

Temp. [°C]	Model	R_g [Ω]	Q_g	C_g [F]	R_{gb} [Ω]	Q_{gb}	C_{gb} [F]	R_e [Ω]	C_e [F]
25	(RQC)(RQC)	1018	$2.487 \cdot 10^{-9}$	$1.146 \cdot 10^{-10}$	815	$4.473 \cdot 10^{-8}$	$5.250 \cdot 10^{-14}$		
50	(RQC)(RQC)	556.8	$6.338 \cdot 10^{-9}$	$1.004 \cdot 10^{-10}$	545	$4.650 \cdot 10^{-8}$	$5.250 \cdot 10^{-14}$		
75	(RQC)(RQC)	276.4	$1.360 \cdot 10^{-8}$	$4.871 \cdot 10^{-11}$	253	$4.484 \cdot 10^{-8}$	$5.250 \cdot 10^{-14}$		
100	(RQC)(RQC)	146.4	$3.551 \cdot 10^{-8}$	$6.431 \cdot 10^{-18}$	93.9	$4.267 \cdot 10^{-8}$	$5.250 \cdot 10^{-14}$		
125	(RQC)(RQC)	52.6	$1.029 \cdot 10^{-6}$	$1.410 \cdot 10^{-8}$	88.61	$5.250 \cdot 10^{-14}$	$5.250 \cdot 10^{-14}$		
150	(RQC)(RQC)(RC)	$1.08 \cdot 10^{9}$	$1.650 \cdot 10^{-15}$	$1.659 \cdot 10^{12}$	$5.61 \cdot 10^{7}$	$3.418 \cdot 10^{-2}$	$5.250 \cdot 10^{-14}$	62.85	$4.01 \cdot 10^{-14}$

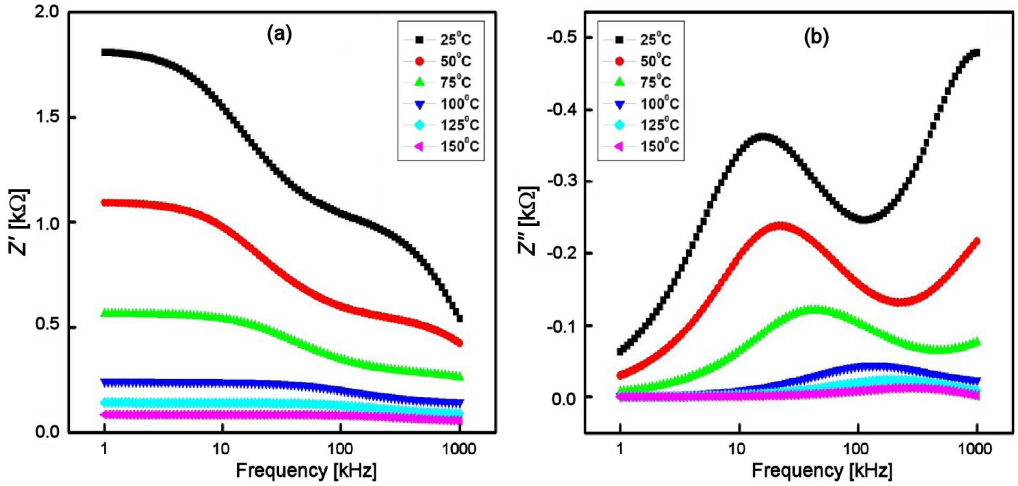

Figure 7. Change of Z' (a) and Z'' (b) with frequency at selected temperature

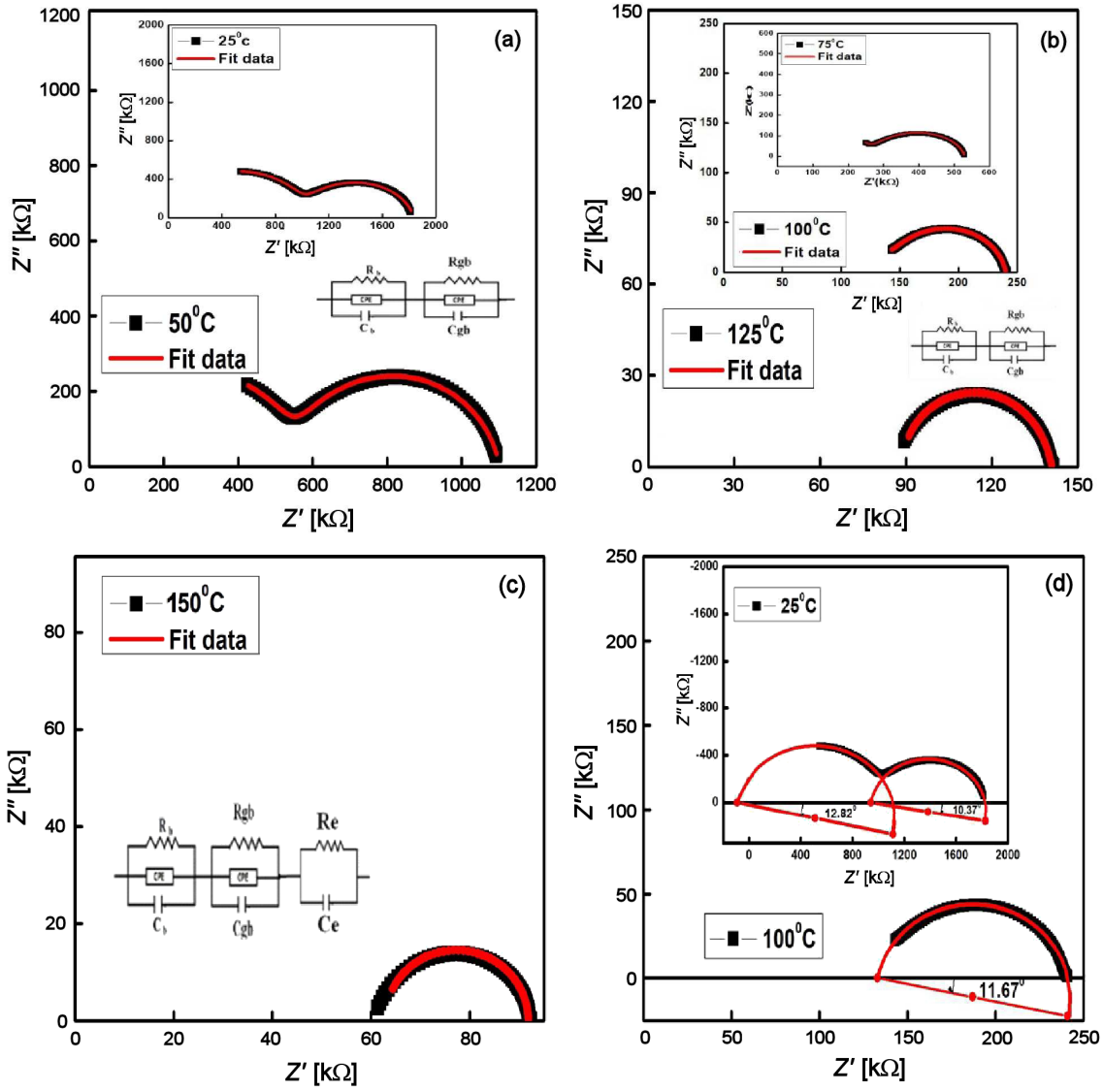

Figure 8. Variation of Z' with Z'' at: a) 25 and 50 °C, b) 75, 100 and 125 °C, c) 150 °C and d) 25 °C and 100 °C with depression angle

ature. Owing to the existence of immobile charges at low temperatures and imperfections/oxygen vacancies at higher temperatures, relaxation process occurs [35].

3.4. Nyquist plots

The Nyquist plots representing the change of Z' with Z'' in the frequency range of 1,kHz–1 MHz and at different temperatures (25–150 °C) is depicted in Fig. 8. The electrode effect, grain and grain boundary are explained by low-frequency, high-frequency and intermediate-frequency independent semicircles respectively, occurring sequentially. The feature of the arc determines the category of relaxation phenomena in the system. An ideal semicircular curve having centre on the Z' axis implies the existence of a single relaxation time and grain identity [36]. The perfect Debye type relaxation corresponds with the coinciding centre of the semicircles with the real impedance axis. An identical circuit of a series combination of parallel resistances (R) and capacitances (C) is operated for individual arc. A disappearance of an ideal Debye type of relaxation can be interpreted by the CPE (constant phase element) which can be connected to the parallel RC system in the proposed circuit [37]. An observed relaxation phenomenon is the non-Debye type due to the imperfections and inhomogeneity of the Nd_2NiMnO_6 sample. For the Debye type relaxation, the test and theoretical data can be determined by using the software ZSIMP WIN version 2.0 [38,39]. In temperature range 25–125 °C, the identical circuit obtained as the combination of two RQC (Q is a constant phase element) circuit and exhibited by two circles representing the contribution from grain and grain boundary effect. For temperature of 150 °C, the equivalent circuit obtained as a series combination of two RQC and one RC circuit describing the contribution from grain and grain boundary effects along with the electrode effect. The non-Debye type relaxation is proved by the deviation of the impedance plane from the real axis by some angle which is shown in Fig. 8d.

3.5. Electrical conductivity

Study of AC conductivity was carried out to find the frequency-dependence of the electrical properties of the material. It also yields knowledge about the behaviour of the charge carriers. AC conductivity (σ_{AC}) was determined by an empirical correlation $\sigma_{AC} = \omega \cdot \varepsilon_r \cdot \varepsilon_0 \cdot \tan\delta$, where ε_0 is the permittivity in vacuum and ω is the angular frequency. For more information about the conduction process in the material we have to proceed with the Jonscher's power law: $\sigma_T = \sigma_{DC} + \sigma_{AC} = \sigma_{DC} + A \cdot T^n$ where σ_{DC} and σ_{AC} are the DC and AC conductivities, respectively. The exponent (n) lies between 0 and 1 which serves as the measure of interaction between mobile ions and lattices, whereas A represents the extent of polarizability [40]. The frequency dependence of AC conductivity (σ_{AC}) has been shown in Fig. 9a. AC conductivity is nearly constant in the low-frequency area, whereas at higher frequencies, diffusion of conductivity is seen. With increment of frequency there is transformation of electrical conductivity from DC (frequency independent) conductivity to AC (frequency dependent) conductivity. The slope change is observed at certain frequency interrelated to polaron hopping of charged basis. With an increment of temperature this hopping frequency shifts towards higher frequency region. The value of $n < 1$ implies the movement associated with translational motion and rapid flow, whereas $n > 1$ implies that the movement is localized, i.e. beyond the species leaving the vicinity. From fitting data, it is realized that the movement of charge carriers in the samples is translational, due to the low value of n (< 1). The values of A and n are given in Table 3. The rise of conductivity with an increment of temperature indicates

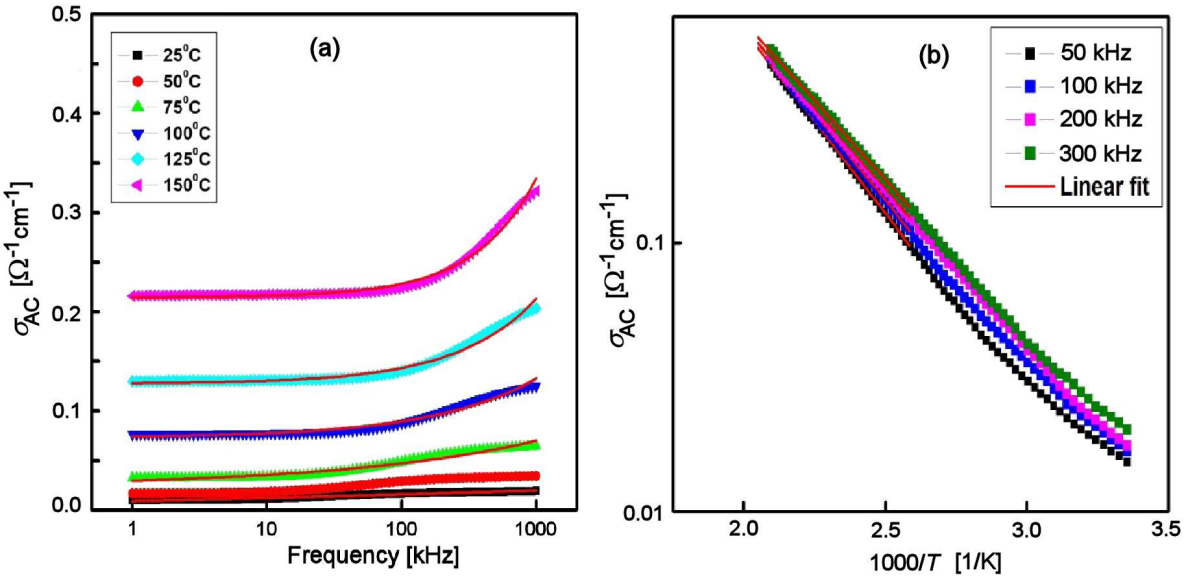

Figure 9. Plot of AC conductivity with frequency at selected temperature (a) and inverse absolute temperature (b)

Table 3. The values of A and n at distinct temperatures for sintered Nd_2NiMnO_6

Temperature [°C]	A	n
25	0.01358	0.02237
50	0.00622	0.0241
75	0.00029	0.02435
100	0.00002	0.02234
125	$9.6836 \cdot 10^{-7}$	0.02113
150	$7.4449 \cdot 10^{-8}$	0.02078

the NTCR nature of the sample [41,42]. The temperature dependence of AC conductivity of the material is depicted in Fig. 9b. The activation energy (E_a) can be determined using the relation:

$$\sigma_{AC} = \sigma_0 \cdot \exp\left(\frac{-E_a}{k_B \cdot T}\right) \tag{8}$$

where all the symbols have their usual meaning. Since the conductivity rises with an increment of temperature, semiconducting behaviour of the material is confirmed. This nature of σ_{AC} promotes the existence of thermally stimulated transport properties in the compound. In the high-temperature region, with the increment of frequency the activation energy reduces. At higher temperatures, the irregularity of polycrystalline samples may be the origin of additional acceptor centres [43]. Thus, the activation energy reduces with the increment of temperature. The calculated values of the activation energies are 0.23, 0.24, 0.25, 0.27 eV at 50, 100, 200 and 300 kHz, respectively. Since dielectric relaxation arises due to the hopping of charge carriers between the Y and Y′ site cations, the estimated activation energy may be used to displace an electron from Ni^{2+} to Mn^{4+}. This activation energy is sufficient for switching over the orientation of polar regions in relaxation process The cause of dielectric relaxation is mostly caused by delocalized carriers in the interaction of Mn^{4+}–O–Mn^{3+} or Ni^{2+}–O–Ni^{3+} and thus make it semiconductor.

3.6. Complex electric modulus studies

To further study the bulk, grain boundary, electrode polarization, electrical conductivity and relaxation process in the material electric modulus has been analysed. This technique yields a vision into the electrical mechanism appearing in the material as a function of temperature and frequency and also helps us to understand the transport mechanism and the relaxation process in the material [44,45]. The other benefit of such technique is to overcome the electrode effect. The graphs of the electric modulus (M' and M'') with frequency are displayed in Figs. 10a and 10b, respectively. The complex electric modulus is given by: $M^* = M' + j \cdot M''$. The value of M' has been calculated by the formula:

$$M' = A\frac{(\omega \cdot R \cdot C)^2}{1 + (\omega \cdot R \cdot C)^2} = A\frac{\omega^2 \cdot \tau^2}{1 + \omega^2 \cdot \tau^2} \tag{9}$$

For all temperatures, M' rises with the increment of frequency. The M' value approximately reaches zero in the low-frequency region indicating the non-existent electrode effect and continuously increases with an increment of frequency. The existence of the induced electric field is not adequate for the restoring force needed for the flow of the charge carriers. Therefore, in the low-frequency region, the value of M' becomes zero, and increases in the high-frequency region. By the continuous dispersion of M' with increment of frequency, the conduction process occurs due to the short range mobility of charge carriers [46]. The increase in M' with the increment of temperature indicates on the temperature dependent relaxation phenomena in the sintered Nd_2NiMnO_6 material. In high-frequency region, the observed tendency of M' to make plateau indicates on the frequency invariant (DC conductivity) electrical properties of the materials.

The value of M'' has been calculated by the formula:

$$M'' = A\frac{\omega \cdot R \cdot C}{1 + (\omega \cdot R \cdot C)^2} = A\frac{\omega \cdot \tau}{1 + \omega^2 \cdot \tau^2} \tag{10}$$

In the Fig. 10b, we observed that with the increment of frequency, value of M'' rises. Obviously, we may expect that above 1 MHz frequency the peak will move to the right (high-frequency region) with an increment of temperature, which is the characteristic of relaxation mechanism.

The temperature dependent complex modulus spectrum (M' *vs.* M'') of the material is depicted in Fig.

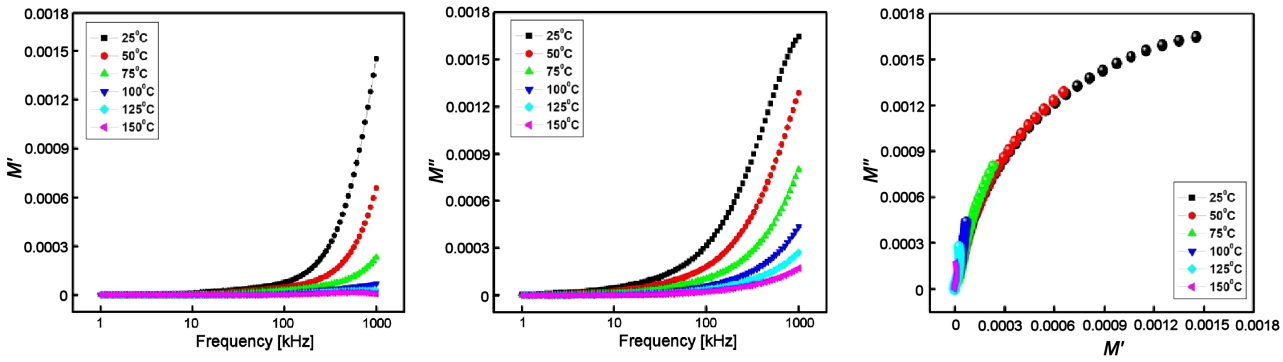

Figure 10. Variation of M' (a) and M'' (b) with frequency and variation of M' with M'' at selected temperature (c)

10c. The arcs obtained at high temperatures are not accurate semicircle(s). The two deformed semi-circles (or their tendency) are obtained representing the existence of both the grain and grain boundary contributions in the sample. These arcs having their centres lying below the real axis indicating non-Debye type of relaxation in the sample [31].

IV. Conclusions

The polycrystalline sample Nd_2NiMnO_6 was synthesized by a high temperature solid state reaction. The monoclinic structure of the sample was found from X-ray analysis. The crystallite size and density of the sample were found to be 41 nm and 4.78 g/cm^3 respectively. The microstructural analysis represents the uniform distribution of grains of different shape and size at the surface of the sample. The electrical parameters are also calculated from dielectric and impedance measurements. In temperature dependence of dielectric property, the dielectric constant increases and at a certain temperature an anomaly was observed. Then the rate of dielectric constant was found to be diminished. The sintered Nd_2NiMnO_6 sample has high dielectric constant due to the combination of conductive grain and insulating grain boundary. The dielectric relaxor behaviour showed by the material agrees with the modified Curie-Weiss law and the Vogel-Fulcher law. From the Nyquist plots for temperatures 25–125 °C, it was found that there is simultaneous occurrence of grain and grain boundary effects represented by the combination of two RQC networks. However, for temperature 150 °C, the equivalent circuit obtained as a series combination of two RQC and one RC circuit describes the contribution from the grain and grain boundary along with electrode effect. The non-Debye type of dielectric relaxation was proved from the study of impedance spectroscopy. The semiconductor behaviour of the sample was obtained in the study of the conductivity versus temperature. The activation energy has been calculated using the Arrhenius equation. The sample Nd_2NiMnO_6 can be used in different modern electronic device applications.

Acknowledgement: The authors would like to extend their gratitude and sincere thanks to Dr. Soobhankar Pati Indian Institute of Technology, Bhubaneswar for providing some experimental facility for microstructure. The use of X-ray diffraction of our central research facility is gratefully acknowledged.

References

1. F. Gheorghiu, L. Curecheriu, I. Lisiecki, P. Beaunier, S. Feraru, M.N. Palamaru, V. Musteata, N. Lupu, L. Mitoseriu, "Functional properties of Sm_2NiMnO_6 multiferroic ceramics prepared by spark plasma sintering", *J. Alloys Compd.*, **649** (2015) 151–158.
2. D.K. Mahato, A. Dutta, T.P. Sinha, "Impedance spectroscopy analysis of double perovskite Ho_2NiTiO_6", *J. Mater. Sci.*, **45** (2010) 6757–6762.
3. R.I. Dass, J. B. Goodenough, "Multiple magnetic phase of $La_2CoMnO_{6-\delta}$ ($0 \leq \delta \leq 0.05$)", *Phys. Rev. B*, **67** (2003) 014401.
4. L. Seixa, A.S. Rodin, A. Carvalho, A.H.C. Neto, "Multiferroic two-dimensional materials", *Phys. Rev. Lett.*, **116** (2016) 206803.
5. M.W. Lufaso, P.W. Barnes, P.M. Woodward, "Structure prediction of ordered and disordered multiple octahedral cation perovskites using SPuDS", *Acta Cryst. B*, **62** (2006) 397–410.
6. G. Blasse, "Ferromagnetic interactions in non-metallic perovskites", *J. Phys. Chem. Solids*, **26** (1965) 1969–1971.
7. A.H. Reshak, S. Azam, "Electronic band structure and specific features of Sm_2NiMnO_6 compound: DFT calculation", *J. Magn. Magn. Mater.*, **342** (2013) 80–86.
8. N.S. Rogado, J. Li, A.W. Sleight, M.A. Subramanian, "Magneto capacitance and magneto resistance near room temperature in a ferromagnetic semiconductor: La_2NiMnO_6", *Adv. Mater.*, **17** (2005) 2225–2227.
9. S.H. Oh, H.Y. Choi, J.Y. Moon, M.K. Kim, Y. Jo, N. Lee, Y.J. Choi, "Nonlinear magneto dielectric effect in double-perovskite Gd_2NiMnO_6", *J. Phys. D: Appl. Phys.*, **48** (2015) 445001.
10. D.C. Sinclair, T.B. Adams, F.D. Morrison, A.R. West, "$CaCu_3Ti_4O_{12}$: One-step internal barrier layer capacitor", *Appl. Phys. Lett.*, **80** (2002) 2153–2155.
11. G. Catalan, "Magneto-dielectric effect without multiferroic coupling", *Appl. Phys. Lett.*, **88** (2006) 102902.
12. Y.S. Koo, T. Bonaedy, K.D. Sung, J.H. Jung, "Magneto-dielectric coupling in core/shell $BaTiO_3/\gamma$-Fe_2O_3 nanoparticles", *Appl. Phys. Lett.*, **91** (2007) 212903.
13. P.M. Tirmali, D.K. Mishra, B.P. Benglorkar, S.M. Mane, S.L. Kadam, S.B. Kulkarni, "Structural, magnetic and dielectric relaxation behaviour study of La_2MnCoO_6 and fully substituted B-site La_2FeCoO_6", *J. Chinese Adv. Mater. Soc.*, **6** (2018) 207–221.
14. F.H. Qing, K.E. Shan Ming, "School of materials science and engineering", *Sci. China Ser. E-Tech. Sci.*, **52** (2009) 2180–2185.
15. F. Calderón-Piñar, O. García-Zaldívar, Y. González-Abreu, "Relaxor behaviour in ferroelectric ceramics", pp. 85–107, Ch. 6 in *Advances in Ferroelectrics*, Ed. by A.P. Barranco. InTech Open, 2012.
16. N. Novak, Z. Kutnjak, "Basic study of relaxors: materials for high technological devices", pp. 275–280 in *Zbornik 4. Študentske konference Mednarodne podiplomske šole Jožefa Stefana*. Ed. by D. Petelin, A. Tavcar, B. Kaluža, Ljubljana, Slovenija: Mednarodna podiplomska šola Jožefa Stefana, 2012.
17. C. Shi, Y. Hao, Z. Hu, "Local valence and physical properties of double perovskite Nd_2NiMnO_6", *J. Phys. D: Appl. Phys.*, **44** (2011) 245405.
18. K. Parida, S. K. Dehury, R.N.P. Choudhary, "Electrical, optical and magneto-electric characteristics of $BiBaFeCeO_6$ electronic system", *Mater. Sci. Eng. B*, **225** (2017) 173–181.
19. V. Purohit, R. Padhee, R.N.P. Choudhary, "Dielectric and impedance spectroscopy of $Bi(Ca_{0.5}Ti_{0.5})O_3$ ceramic", *Ceram. Int.*, **44** (2018) 3993–3999.
20. S. Hajra, S. Sahoo, R. Das, R.N.P. Choudhary, "Structural, dielectric and impedance characteristics of $(Bi_{0.5}Na_{0.5})TiO_3$-$BaTiO_3$ electronic system", *J. Alloys Compd.*, **750** (2018) 507–514.

21. O.F. Mossoti, *Mem. di Mathem e.di.fisica in Modena*, **24** (1850) 49.
22. T. Siritanon, N. Chathirat, C. Masingboon, T. Yamwong, S. Maensiri, "Synthesis, characterization, and dielectric properties of Y_2NiMnO_6 ceramics prepared by a simple thermal decomposition route", *J. Mater. Sci.: Mater. Electron.*, **25** (2014) 1361–1368.
23. C.W Tai, K.Z Baba-Kishi, "Relationship between dielectric properties and structural long-range order in $(x)Pb(In_{1/2}Nb_{1/2})O_3$:$(1-x)Pb(Mg_{1/3}Nb_{2/3})O_3$ relaxor ceramics", *Acta Mater.*, **54** (2006) 5631–5640.
24. A.E. Glazounov, A.K. Tagantsev, "Direct evidence for Vögel-Fulcher freezing in relaxor ferroelectrics", *Appl. Phys. Lett.*, **73** (1998) 856–858.
25. S. Mitra, A.R. Kulkarni, "Synthesis and electrical properties of new lead-free $(100-x)(Li_{0.12}Na_{0.88})NbO_3$–$xBaTiO_3$ $(0 \leq x \leq 40)$ piezoelectric ceramics", *J. Am. Ceram. Soc.*, **99** (2016) 888–895.
26. B. Tilak, "Ferroelectric relaxor behavior and spectroscopic properties of Ba^{2+} and Zr^{4+} modified sodium bismuth titanate", *Am. J. Mater. Sci.*, **2** [4] (2012) 110–118.
27. M.R. Panigrahi, S. Panigrahi, "Phase transition and dielectric study in $Ba_{0.95}Dy_{0.05}TiO_3$ ceramic", *Bull. Mater. Sci.*, **34** [4] (2011) 927–931.
28. T. Badapanda, S.K. Rout, S. Panigrahi, E. Sinha, T.P. Sinha, "Ferroelectric phase transition of $Ba_{1-x}Sr_xTi_{0.6}Zr_{0.4}O_3$ ceramics", *Phase Transitions*, **81** (2008) 897–906.
29. R.I. Dass, J-Q. Yan, J.B. Goodenough, "Oxygen stoichiometry, ferromagnetism, and transport properties of $La_{2-x}NiMnO_{6+\delta}$", *Phys. Rev. B*, **68** (2003) 064415.
30. B.E. Vugmeister, M.D. Glinichuk, "Dipole glass and ferroelectricity in random-site electric dipole systems", *Rev. Mod. Phys.*, **62** (1990) 993–1026.
31. R. Ranjan, R. Kumar, N. Kumar, B. Behera, R.N.P. Choudhary, "Impedance and electric modulus analysis of Sm-modified $Pb(Zr_{0.55}Ti_{0.45})_{1-x/4}O_3$ ceramics", *J. Alloys Compd.*, **509** (2011) 6388–6394.
32. A. Rouahi, A. Kahouli, F. Challali, M.P. Besland, C. Vallée, B. Yangui, S. Salimy, A. Goullet, A. Sylvestre, "Impedance and electric modulus study of amorphous TiTaO thin films: Highlight of the interphase effect", *J. Phys. D: Appl. Phys.*, **46** (2013) 065308.
33. M. Idrees, M. Nadeem, M.M. Hassan, "Investigation of conduction and relaxation phenomena in $LaFe_{0.9}Ni_{0.1}O_3$ by impedance spectroscopy", *J. Phys. D: Appl. Phys.*, **43** (2010) 155401.
34. M. Ahmad, M.A. Rafiq, Z. Imran, K. Rasool, R.N. Shahid, Y. Javed, M.M. Hasan, "Charge conduction and relaxation in MoS_2 nanoflakes synthesized by simple solid state reaction", *J. Appl. Phys.*, **113** [4] (2013) 043704–043706.
35. K. Parida, S.K. Dehury, R.N.P. Choudhary, "Structural, electrical and magneto-electric characteristics of complex multiferroic perovskite $Bi_{0.5}Pb_{0.5}Fe_{0.5}Ce_{0.5}O_3$", *J. Mater. Sci. Mater. Electron.*, **27** (2016) 11211–11219.
36. D.C. Sinclair, A.R. West, "Impedance and modulus spectroscopy of semiconducting $BaTiO_3$ showing positive temperature coefficient of resistance", *J. Appl. Phys.*, **66** (1989) 3850.
37. S. Sahoo, P.K. Mahapatra, R.N.P. Choudhary, "The structural, electrical and magnetoelectric properties of soft-chemically-synthesized $SmFeO_3$ ceramics", *J. Phys. D: Appl. Phys.*, **49** (2016) 035302.
38. S.K. Dehury, K. Parida, R.N.P. Choudhary, "Dielectric, impedance and magneto-electric characteristics of $Bi_{0.5}Sr_{0.5}Fe_{0.5}Ce_{0.5}O_3$ electronic material", *J. Mater. Sci.: Mater. Electron.*, **28** (2017) 10441–10448.
39. B. Garbarz-Glos, W. Bąk, M. Antonova, M. Pawlik, "Structural, microstructural and impedance spectroscopy study of functional ferroelectric ceramic materials based on barium titanate", *IOP Conf. Ser.: Mater. Sci. Eng.*, **49** (2013) 012031.
40. K.D. Chandrasekhar, A.K. Das, C. Mitra, A. Venimadhav, "The extrinsic origin of the magnetodielectric effect in the double perovskite La_2NiMnO_6", *J. Phys.: Condens. Matter*, **24** (2012) 495901.
41. N. Panda, B.N. Parida, R. Padhee, R.N.P. Choudhary, "Dielectric and electrical properties of the double perovskite $PbBaBiNbO_6$", *J. Electron. Mater.*, **44** (2015) 4275–4282.
42. S. Dash, R. Padhee, P.R. Das, R.N.P. Choudhary, "Enhancement of dielectric and electrical properties of $NaNbO_3$-modified $BiFeO_3$", *J. Mater. Sci.: Mater. Electron.*, **24** (2013) 3315–3323.
43. F. Mebarki, E. David, "Characterization of the dielectric endurance of reinforced recycled PET using electro-thermal aging test", *IEEE Trans. Dielectr. Electr. Insul.*, **22** [6] (2015) 3513–3520.
44. B.N. Parida, N. Panda, R. Padhee, P.R. Das, R.N.P. Choudhary, "Dielectric relaxation and impedance analysis of ferroelectric double perovskite Pb_2BiNbO_6", *J. Mater. Sci.: Mater. Electron.*, **28** (2017) 1824–1831.
45. B. Pati, R.N.P. Choudhary, P.R. Das, "Phase transition and electrical properties of strontium orthovanadate", *J. Alloys Compd.*, **579** (2013) 218–226.
46. S. Pattanayak, R.N.P. Choudhary, "Synthesis, electrical and magnetic characteristics of Nd-modified $BiFeO_3$", *Ceram. Int.*, **41** (2015) 9403–9410.